Slipstream Deformation of a Propeller-Wing Combination Applied for Convertible UAVs in Hover Condition

Y. Leng*, M. Bronz, T. Jardin and J-M. Moschetta
ISAE-SUPAERO, Université de Toulouse, France
ENAC, Université de Toulouse, France

ABSTRACT

Convertible unmanned aerial vehicle (UAV) promises a good balance between convenient autonomous launch/recovery and efficient long range cruise performance. Successful design of this new type of aircraft relies heavily on good understanding of powered lift generated through propeller-wing interactions, where the velocity distribution within propeller slipstream is critical to estimate aerodynamic forces during hover condition. Current study analysed a propeller-wing combination with a plain flap. A 5-hole probe measurement system was built to construct 3 dimensional velocity field at a survey plane after trailing edge. The study has found that significant deformation of propeller slipstream was present in the form of opposite transverse displacement on extrados and intrados. The deformation could be enhanced by flap deflections. Velocity differences caused by the slipstream deformation could imply local variation of lift distribution compared to predictions from conventional assumptions of cylindrical slipstream. The research underlined that the mutual aspect of propeller-wing interaction could be critical for low-speed aerodynamic design.

1 INTRODUCTION

Small-scale unmanned aerial vehicle has recently attracted great amount of interests due to their autonomous capability to conduct highly repetitive or dangerous flight missions. This capability is realised through electrical propulsion system and improved autoflight system. The current UAV lifting systems are generally derived by down-scaling manned aircraft. The clear division of rotorcraft and fixed-wing aircraft can still be seen in most professional UAV applications.

It has been seen however that a hybrid design that combines the vertical take-off / landing capability and the efficiency of fixed-wing aircraft could improve mission performance of current UAV applications and eventually open up new type of missions. Rotor lifting system is inefficient for long-endurance flight, and thus mission range is limited. On the other hand, most current fixed-wing UAVs rely on crew and sometimes specific systems for launch and recovery, which limits the origin and destination to dedicated points where the aircraft can be accommodated by ground crew. To perform a fully autonomous long-range mission, a hybrid design called convertible drone is needed.

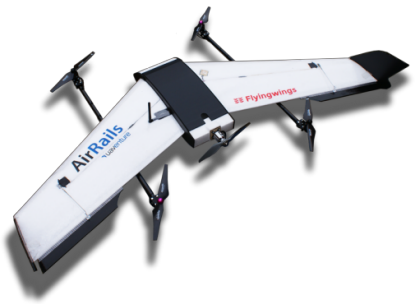

(a) Combination of quad-copter and flying wing [1]

(b) Darko developped by ENAC drone research group

Figure 1: Examples of convertible drone configurations

The key to an optimised design of convertible drone lies in the interaction between propulsion system and the lifting surfaces. An entirely independent design, such as shown in Figure 1a requires lifting propellers that aren't used in cruise flight, hence additional weight and drag are introduced. A

*Email address(es): yuchen.leng@isae-supaero.fr

fully hybrid approach (Figure 1b) takes advantage of arranging lifting surfaces within propeller slipstream for augmented lift from blown wing. In this way the propeller and wing are both used during hover and cruise flight, and their sizes must match to deliver the required aerodynamic performance while minimizing the weight of combined system.

Unlike an independent design, the hover lift is distributed between the vertical component of propeller thrust and wing lift augmented by rotor slipstream. Thus flow interference between the wing and slipstream must be well understood to ensure sufficient lift in hover.

To further augment wing lift and to provide flight control, trailing edge flap is typically installed, such as shown in Figure 2. Propeller slipstream can therefore be deflected at a certain angle to generate additional aerodynamic force and moment. Sufficient pitch and roll control authority can be achieved with appropriate flap design.

Figure 2: Convertible UAV Cyclone hovering with negative flap deflection

During preliminary design, reduced-order models such as panel method, vortex lattice method, to name a few, are preferred due to their capability of analysing large amount of candidate configurations at a relatively small computational cost [2]. Veldhuis et al. has identified two approaches in analysing propeller-wing systems : single approach and dual-coupling approach.

In single analysis mode, only the influence of propeller slipstream is taken into consideration. When calculating wing lift for sections immersed in propeller slipstream, the accelerated freestream velocity and sometimes the circumferential swirl velocity are applied to calculate local angle of attack and dynamic pressure. The velocities in the slipstream are computed from a free propeller model, such as one based on blade element momentum theory.

A dual-coupling mode is sometimes used to improve accuracy. The same calculation on wing sections still applies. A main difference is that the freestream condition of the propeller is also modified after the wing circulation distribution is solved, and induced velocity from the lifting surfaces is added to flight speed for propeller calculation. Ideally, an iterative approach is used until both solutions converge.

Both analysis modes require an empirical coefficient to attenuate propeller induced velocity before application in wing calculation [3, 4]. This suggests propeller induced velocity distribution might have changed due to the presence of wing. The effect was treated semi-empirically in [3], but a clear physical understanding is still absent.

Recent studies on tractor propeller wake measurements have found that the influence of wing to the propeller isn't limited to the flow upstream of the rotor disk. Deters et al [5] have used a seven-hole probe to make wake survey at different downstream locations after three different propellers. A flat plate wing is situated close to the propeller. The presence of wing is significant that the upper and lower halves of the slipstream translated in opposite direction by a distance up to 1 propeller radius at survey plane. The phenomenon was first observed and analysed by Witkowski et.al [6]. However neither studies provided quantitative analysis.

In this paper, a wake survey in static condition is presented at different rotation speeds and flap deflection angles. The test equipment and condition will be introduced in Section 2. Results and quantitative analysis will be shown in Section 3.

The test was also performed with flap deflection to investigate the slipstream development when the wing was generating lift.

2 TEST SET-UP

2.1 Test equipments

The test was conducted in the indoor flight arena at Ecole National de l'Aviation Civile (ENAC). The flight arena's volume provides static ambient environment for simulating hover condition.

The test equipments were divided into three subsystems : 1) propeller-wing combination and their relevant motion control system ; 2) 5-hole probe and its data acquisition system ; 3) motion control system for 5-hole probe. The test setup in shown in Figure 3.

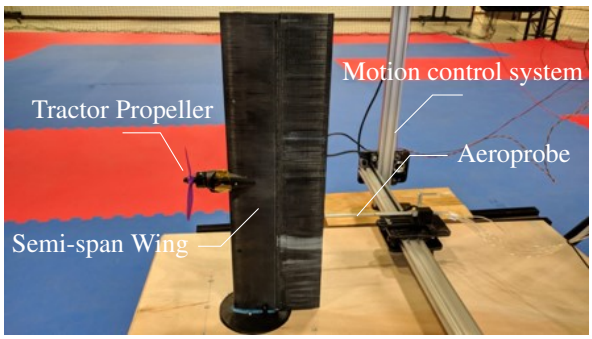

Figure 3: Test set-up in ENAC indoor flight arena

2.1.1 Propeller-wing model

The wing tested was a semi-span model with $500mm$ span. The straight wing had a constant chord length of $150mm$ and NACA0012 aerofoil section. A propeller nacelle was situated at $55mm$ from plane of symmetry, where a CM2206 direct current brushless motor was enclosed. A full-span plain flap was installed for the last 50% chord, and a servo allowed symmetrical flap deflection of $15°$ in either direction.

An APC 3-blade 5x4.6E propeller was tested. A tilt-rotor mechanism was designed to allow propeller install angle to change between $-10°$ to $10°$ with respect to wing chord line. The tilt mechanism was fixed at $0°$ for this experiment.

2.1.2 5-hole probe

The wake survey was conducted with an Aeroprobe 5-hole probe. The centre of probe head was located at $15mm$ behind trailing edge or 1.7 times propeller diameters downstream of rotor plane.

At the centre sphere, five holes were arranged in a cross pattern with one in the centre, a pair in vertical plane and another pair perpendicularly arranged. A series of static ports were situated after the probe head. When air is blown, the velocity, pitch and yaw attitude of probe will produce pressure difference between centre hole and static ports, vertical pair and side pair holes.

Honeywell analogue differential pressure sensors were used to measure the three pairs of pressure differences which were needed to resolve flow velocity. A calibration method proposed by Reichert et al [7] were used to take into consideration of cross-product terms and to correct alignment errors.

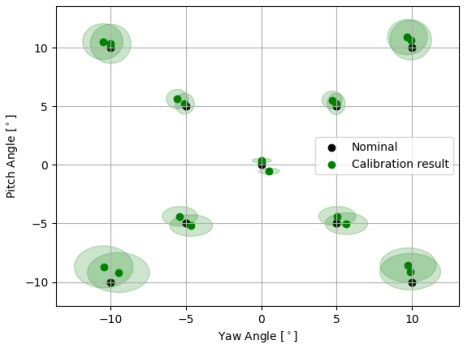

Figure 4: Flow angle measurement

The calibration were also analysed for measurement error. An uncertainty analysis were performed similar to the one described by Reichert et al, and fitting error as well as pressure fluctuations were considered in uncertainty propagation. A validation test were performed in the wind tunnel with known wind velocity and probe attitude. Flow angle measurement and its uncertainty is plotted in figure 4; flow speed measurement and its uncertainty is plotted in figure 5.

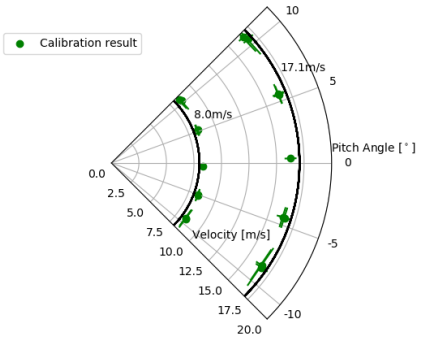

Figure 5: Flow speed measurement

From the validation case, uncertainty in flow speed was estimated at $\pm 0.3m/s$ and error in flow angle was estimated to be less than $2°$ below $20°$.

2.1.3 Motion control system

A 2-axis linear motion frame was constructed to allow automatic wake survey at a given plane perpendicular to propeller axis. Three stepper motors controlled by I2C bus were used to move a cart on which the 5-hole probe was mounted within the survey plane. The measurement was made on a 15×15 grid using alternating survey pattern as depicted in figure 6. Mean velocity data was obtained from sample recorded at $700Hz$ over a period of $5s$.

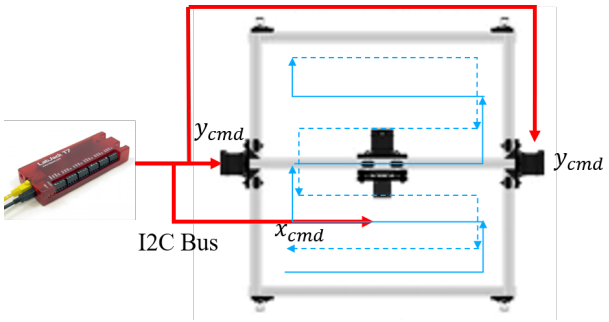

Figure 6: Motion control system and survey pattern

2.2 *Test conditions*

All tests were conducted at $V_\infty = 0$ to analyse flow condition at hover flight. Different propeller rotation speed and flap angle were tested, and the test matrix is given in Table 1

The rotation of propeller in front of a finite wing made the situation no longer symmetrical. Since lift must vanish at wing tip, spanwise lift distribution isn't uniform for a finite wing without propeller. Furthermore, an up-going propeller blade influences the wing section behind in a different

Test Variables	
Rotation Speed [rpm]	5770 / 8000 / 10000
Flap Deflection [°]	0, $\pm$15

Table 1: Test Parameters

way from the down-going blade, hence the influence of a single rotating propeller isn't symmetrical. For this reason, both positive and negative flap deflections were tested.

3 RESULTS

In this section the results of 0° flap deflection will first be presented in subsection 3.1, where the effect of rotation speed as well as the general flow structure of propeller-wing interference will be discussed. Further discussion will continue in subsection 3.2 on the effect of flap deflection.

3.1 0° Flap Deflection

The configuration at neutral flap setting excluded the effect of different velocity and pressure profiles on the extrados and intrados. The wake survey therefore was only influenced by the fact that propeller slipstream was separated by a solid surface.

The wake survey at $8000rpm$ is presented in Figure 7. The velocity field distribution in the survey plane is depicted as two components : the streamwise component u is perpendicular to the survey plane and the transverse component $V_t = \sqrt{v^2 + w^2}$ is situated within the survey plane. In Figure 7, the background contour shows u distribution while the transverse V_t is superposed by arrow symbols that give both magnitude and direction of V_t at sample points.

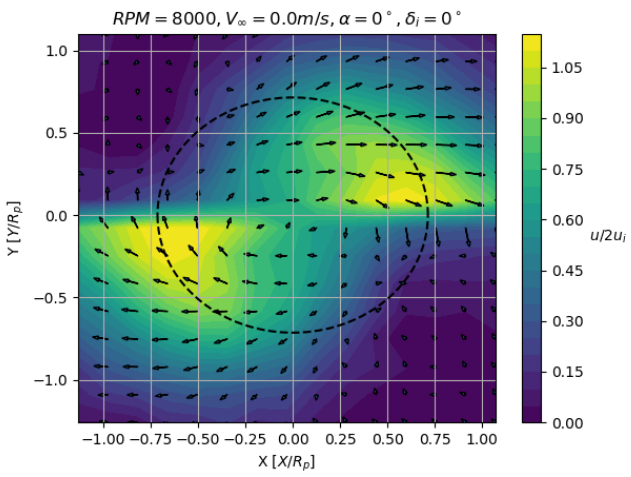

Figure 7: Velocity distribution at survey plane for symmetrical configuration at $8000rpm$

Above and below the wing, propeller slipstream can be identified as a semi-circular region of high energy airflow. Within the slipstream, both u and V_t are noticeably higher in magnitude than the surrounding flow region. The increase in axial velocity is expected as the propeller produces forward thrust by accelerating air in downstream direction. The transverse velocity is caused by the air resistance against blade rotation. Transverse velocity contains both induced velocity and viscous effect, and is commonly referred to as swirl in rotary wing terminology.

According to momentum theory [8], the induced axial velocity at propeller disk can be related to thrust coefficient.

$$u_i = nD\sqrt{\frac{2C_T}{\pi}} \tag{1}$$

where n is rotation speed in revolution per second and D is propeller diameter. Thrust coefficient is defined as $C_T = \frac{T}{\rho n^2 D^4}$, and was obtained as tabulated data from propeller manufacturer at different rotation speeds [9]. After the rotor plane, contraction of slipstream accelerates flow towards twice of u_i at downstream infinity. The flow survey is non-dimensionalised using the induced axial velocity at ultimate wake. The benefit of such normalisation is to remove the effects of thrust loading and rotational speed.

A circle in dashed line represents the undisturbed slipstream boundary obtained from vortex theory from McCormick [10], where

$$R(\bar{z}) = R_p\sqrt{1 + \bar{z}^2 - \bar{z}\sqrt{1 + \bar{z}^2}} \tag{2}$$

where $\bar{z}$ is the distance from propeller plane normalized by R_p and $\bar{z}$ is negative downstream. Through comparison with the actual high-speed regions, a distinct separation of flow structures between the extrados and intrados can be observed.

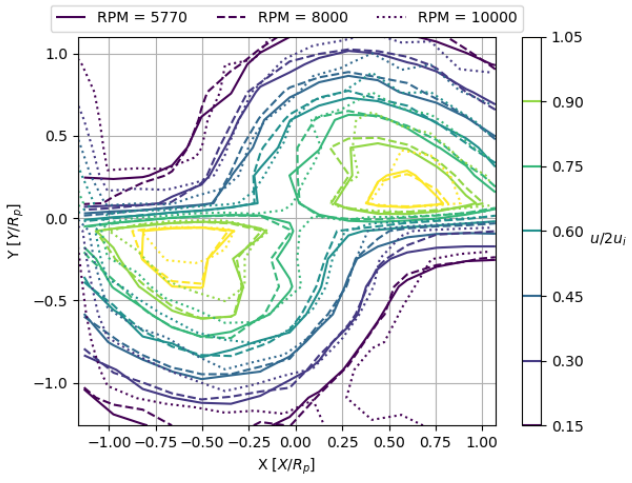

Figure 8: Comparison of axial velocity distribution at different rotation speeds

While increases in u_i and V_t can be reasonably explained by free propeller theory, movement of the two slipstream re-

gions can't be similarly explained. For a single propeller, the slipstream will stay together as in an approximate cylindrical shape. But when a wing is present, as seen in Figure 7, the upper slipstream exhibited a general displacement towards the right (outboard) while the lower slipstream region moves oppositely towards the left (inboard). The directions of movement is associated with the direction of propeller, where in the test case, the inboard blade was turning upward relative to the wing chord.

Axial velocity contours of cases from three different rotation speeds are plotted in Figure 8, where the solid line depicts u distribution at $5770rpm$, dashed line represents the one at $8000rpm$ and dotted line is for $10000rpm$.

Plotted in non-dimensional form, the contour lines of three different cases generally overlap for most flow region. Major differences lie close to the axial velocity peaks at intrados and extrados. The general agreement of flow topology suggests that at hover condition, the wake development is scalable with thrust loading and blade rotation.

A quantifiable measurement is made by determining the centres of extrados and intrados slipstreams. Due to the presence of wing wake, the slipstream centre cannot be easily defined. An indirect method was used to determine slipstream centre through shear stress at the boundary.

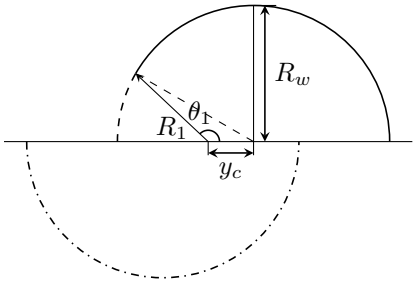

Figure 9: Geometry relations to determine slipstream centre

From turbulent jet theory, it can be concluded that the axial velocity profile of a round jet surrounded by static air can be approximated by Gaussian function. The jet boundary corresponds to where the extrema of shear stress exists. If streamwise partial derivatives ($\frac{\partial}{\partial x}$) are assumed to be small compared to cross flow derivatives, the cross-flow shear stress can therefore be determined.

$$\tau_{xy} = \mu \frac{\partial u}{\partial y} \tag{3}$$

$$\tau_{xz} = \mu \frac{\partial u}{\partial z} \tag{4}$$

The wake boundary was then determined to be the locus of maximum transverse shear stress, drawing analogy from conclusions of turbulent jet theory.

$$(y, z) : max \sqrt{\tau_{xy}^2 + \tau_{xz}^2} \tag{5}$$

The vertical extrema of the slipstream boundary were chosen as the radius of contracted wake R_w. The angular and radial position of the closest points of slipstream boundary to rotational axis were determined as R_1 and θ_1. From geometry relations, the slipstream centre can then be determined.

$$y_c = \sqrt{R_w^2 - (R_1 \sin\theta_1)^2} + R_1 \cos\theta_1 \tag{6}$$

The displacement of slipstream centre from propeller axis can therefore be found, and the results for three test cases can be found in Table 2.

RPM	C_T	y_c/R	Theoretical y_c/R	Error
5770	0.1907	0.4290	0.4252	0.9%
8000	0.1908	0.4086	0.4253	3.9%
10000	0.1906	0.4017	0.4252	5.5%

Table 2: Centreline displacement at different rotation speeds

$$\bar{y}_c(\bar{z}) = \begin{cases} 0, & \bar{z}_{LE} \le \bar{z} \\ \frac{2}{\pi}(\tan\phi - \sec\phi)(\bar{z} - \bar{z}_{LE}) & \bar{z}_{TE} \le \bar{z}, \\ \quad -\frac{2}{\pi}\sec\phi\left(\sqrt{1+\bar{z}^2} - \sqrt{1+\bar{z}_{LE}^2} + \ln\left|\frac{\bar{z}_{LE}}{\bar{z}}\frac{1-\sqrt{1+\bar{z}^2}}{1-\sqrt{1+\bar{z}_{LE}^2}}\right|\right), & \bar{z} < \bar{z}_{LE} \\ \frac{2}{\pi}(\tan\phi - \sec\phi)(\bar{z}_{TE} - \bar{z}_{LE}) & \\ \quad -\frac{2}{\pi}\sec\phi\left(\sqrt{1+\bar{z}_{TE}^2} - \sqrt{1+\bar{z}_{LE}^2} + \ln\left|\frac{\bar{z}_{LE}}{\bar{z}_{TE}}\frac{1-\sqrt{1+\bar{z}_{TE}^2}}{1-\sqrt{1+\bar{z}_{LE}^2}}\right|\right) & \bar{z} < \bar{z}_{TE} \\ \quad +\frac{2}{\pi}\left[\tan\phi(\bar{z} - \bar{z}_{LE}) - \frac{\bar{z} - \bar{z}_{TE}}{\bar{z}_{TE}\left(\sqrt{1+\bar{z}_{TE}^2} - \bar{z}_{TE}^2\right)}\sec\phi\right], & \end{cases} \tag{7}$$

From Table 2 it can be concluded that the three cases have nearly identical wake displacement. A theoretical result was also calculated for each case. This value is based on a potential flow method considering the mean chord surface as an imaginary plane, and thus a transverse velocity is induced from streamwise vortices in propeller slipstream, such idea was first introduced in [6] qualitatively and a quantitative model has been proposed by Leng et al [11].

The resulting model for centreline displacement $\bar{y}_c = y_c/R$ is a function of downstream location $\bar{z} = z/R$, with blade tip vortex shedding angle ϕ as a parameter. The centreline displacement is given in equation 7 at static condition.

Angle ϕ can be calculated from momentum theory using thrust coefficient, and $\bar{z}_{LE}$, $\bar{z}_{TE}$ are leading edge and trailing edge locations divided by propeller radius with origin at rotor centre and negative direction pointing downstream.

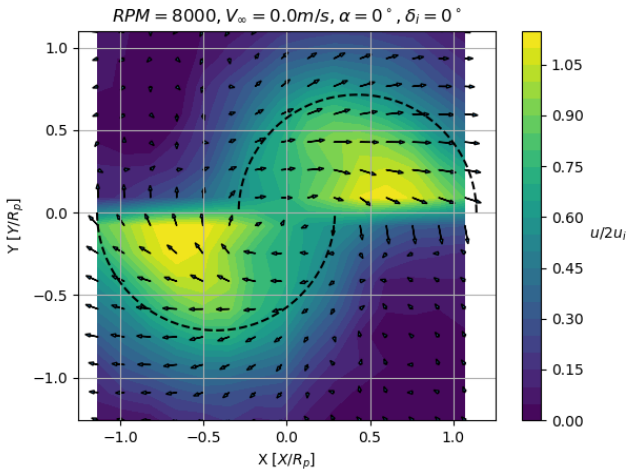

Figure 10: Velocity distribution at survey plane for symmetrical configuration at $8000rpm$, with displaced slipstream boundary

In Figure 10, slipstream boundary from momentum theory was displaced by the predicted amount from Table 2. The deformed boundary appeared to include both high-speed flow regions at extrados and intrados. The results confirm that at static condition, displaced centreline can be accurately calculated using the theoretical model. The results seem to affirm that the presence of wing serves as an imaginary plane for slipstream vortex system, and its induced transverse velocity component explains centreline displacement.

3.2 Effect of Flap Deflection

In subsection 3.1 the slipstream development in $0°$ flap deflection configuration was presented and analysed. In this condition the wing wasn't lifting, and thus the transverse slipstream displacement was purely caused by the presence of solid surface between the extrados and intrados parts of slipstream.

Results obtained at $8000rpm$ are included and discussed in this section, while the other results are included in appendix for simplicity. The effects discussed in this section are similar at a different tested rotation speed.

Figure 11 demonstrated the wake survey in a similar fashion as in Figure 7. The dashed line represents the flap trailing edge location when deflected. High speed region can still be observed in the velocity field, but the distribution took a different shape because of the deflection of flap. Besides the transverse displacement in left and right directions, the slipstream profiles also differ from each other in their vertical expansion. On the extrados, the slipstream was displaced towards the right and took a slightly narrower width. While the highest point of extrados slipstream stayed close to 1 propeller radius, the region spread lower and generally followed the deflected trailing edge flap. The extended vertical expansion is consistent with the reduced lateral width, since flow continuity must be satisfied.

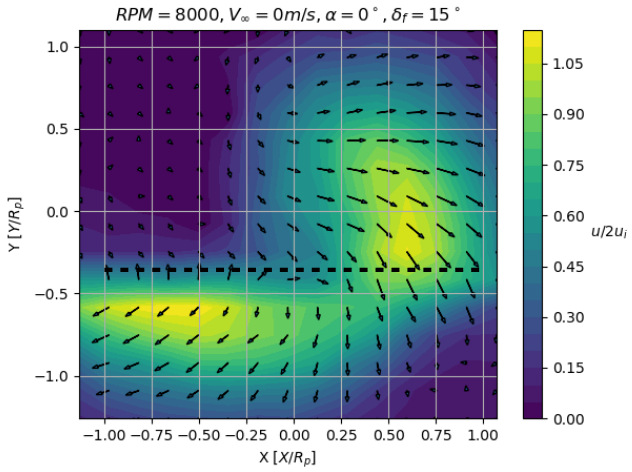

Figure 11: Velocity distribution at survey plane for with $15°$ flap deflection at $8000rpm$

The intrados slipstream was wider and flatter compared to the extrados slipstream and Figure 7. The combined effect produced a distinct velocity difference for the wing section after up-going blade (inboard section), while such difference was more subtle on the other side. The non-uniform velocity distribution could imply significant local lift variation in the surveyed section.

Wake survey for negative flap deflection is depicted in Figure 12. The velocity distribution is generally axial symmetric of Figure 11. However the vertical extent of the intrados slipstream is slightly larger than the extrados slipstream in positive flap deflection. In Figure 12, the wake boundary of intrados slipstream is shown lower than 1 propeller radius.

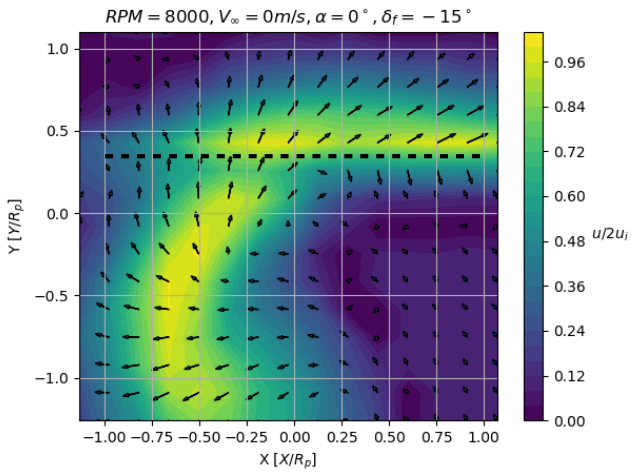

Figure 12: Velocity distribution at survey plane for with $-15°$ flap deflection at $8000rpm$

4 CONCLUSION

In this paper, a wake survey was presented immediately after a propeller-wing combination to investigate the flow interaction for a convertible UAV under hover condition. A symmetric wing profile was tested in ENAC indoor flight arena at calm wind condition. Velocity magnitude and direction were measured by a 5-hole probe at a plane perpendicular to streamwise direction and downstream of trailing edge. The test was conducted with zero flap deflection, as well as with flap deflection of $15°$ in either direction.

The results demonstrated that the presence of wing influences velocity distribution within propeller slipstream compared to a free propeller. In the experiment, the upper half slipstream was observed to translate towards outboard while the lower half slipstream translates towards inboard. The results contrast with most reduced-order model of propeller-wing interaction where propeller wake was assumed to keep its cylindrical shape.

Comparison with a theoretical model suggests that wing influence on propeller slipstream velocity distribution can be accurately modelled using method of reflection on slipstream streamwise vorticity.

The influence of wing on velocity distribution within slipstream was observed to be different between upper and lower surfaces when flap deflection was present, with the deformation being stronger on the wing surface opposite to flap deflection.

REFERENCES

[1] Quadplane. `http://uaventure.com/fcs/`, [Online; accessed 31-July-2019].

[2] LLM Veldhuis. Review of propeller-wing aerodynamic interference. In *24th International Congress of the Aeronautical Sciences*, volume 6, 2004.

[3] Gavin Kumar Ananda Krishnan, Robert W Deters, and Michael S Selig. Propeller-induced flow effects on wings of varying aspect ratio at low reynolds numbers. In *32nd AIAA Applied Aerodynamics Conference*, page 2152, 2014.

[4] Kitso Epema. Wing Optimisation for Tractor Propeller Configurations: Validation and Application of Low-Order Numerical Models Adapted to Include Propeller-Induced Velocities. Master's thesis, Delft University of Technology, Delft, Netherlands, 2017.

[5] Robert W Deters, Gavin K Ananda, and Michael S Selig. Slipstream measurements of small-scale propellers at low reynolds numbers. In *33rd AIAA Applied Aerodynamics Conference*, page 2265, 2015.

[6] Dave P Witkowski, Alex KH Lee, and John P Sullivan. Aerodynamic interaction between propellers and wings. *Journal of Aircraft*, 26(9):829–836, 1989.

[7] Bruce A. Reichert, Bruce J. Wendt, and United States. *A new algorithm for five-hole probe calibration, data reduction, and uncertainty analysis*. National Aeronautics and Space Administration ; National Technical Information Service, distributor [Washington, DC] : [Springfield, Va, 1994.

[8] Gordon J Leishman. *Principles of helicopter aerodynamics with CD extra*. Cambridge university press, 2006.

[9] Apc propeller performance data. `https://www.apcprop.com/technical-information/performance-data/`, [Online; accessed 21-May-2019].

[10] B.W. McCormick. *Aerodynamics, Aeronautics, and Flight Mechanics*. Wiley, 1994.

[11] Yuchen Leng, Murat Bronz, Thierry Jardin, and Jean-Marc Moschetta. Comparisons of different propeller wake models for a propeller-wing combination. In *8th European Conference for Aeronautics and Space Sciences*, 2019.

APPENDIX A: WAKE SURVEYS WITH FLAP

Wake surveys with $\pm 15^{\circ}$ flap deflections are depicted in Figure 13a and Figure 13b for propeller rotation speed at $5770rpm$.

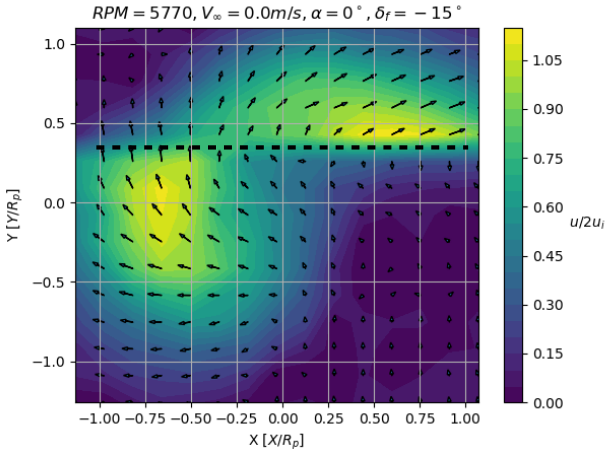

(a) -15° flap deflection

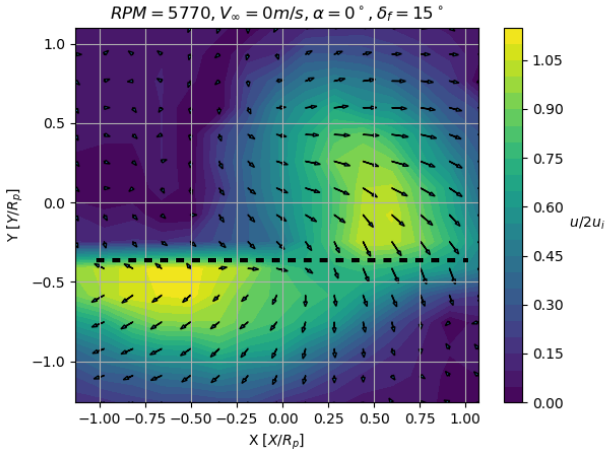

(b) 15° flap deflection

Figure 13: Velocity distribution at survey plane for with flap deflections at $5770rpm$

Wake surveys with $\pm 15^{\circ}$ flap deflections are depicted in Figure 14a and Figure 14b for propeller rotation speed at $10000rpm$.

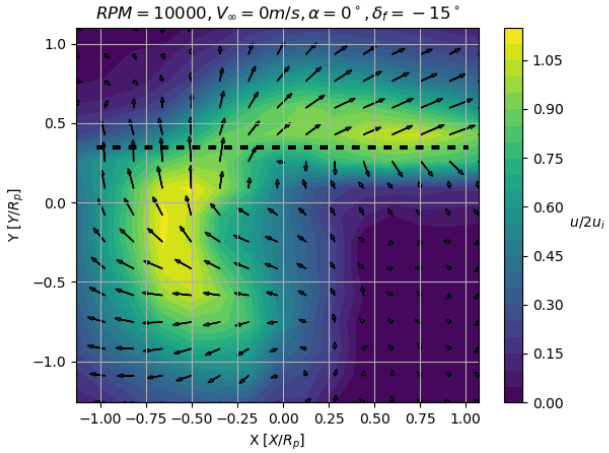

(a) -15° flap deflection

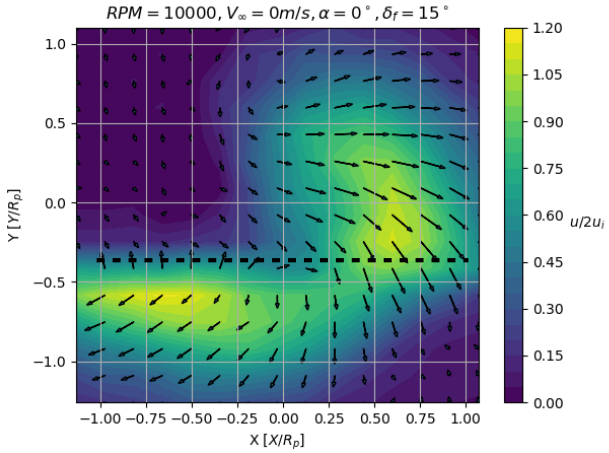

(b) 15° flap deflection

Figure 14: Velocity distribution at survey plane for with flap deflections at $10000rpm$